

Mechanism of Coordinated Gating and Signal Transduction in Purine Biosynthetic Enzyme Formylglycinamide Synthetase

Nandini Sharma, Sukhwinder Singh,[§] Ajay S. Tanwar,[§] Jagannath Mondal, and Ruchi Anand*



Cite This: *ACS Catal.* 2022, 12, 1930–1944



Read Online

ACCESS |



Metrics & More



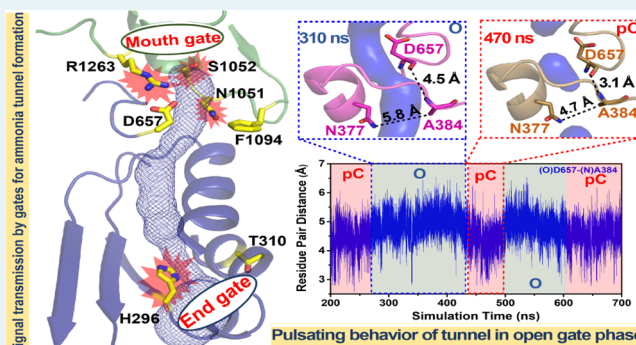
Article Recommendations



Supporting Information

ABSTRACT: Enzymes that harbor transient tunnels have a complex interplay of allostery that links their assembly/disassembly with the catalytic cycle. Here, by employing PurL, a purine biosynthetic enzyme, as a model system, we decipher the mechanism of catalytic coupling, precise orchestration of signal transduction, associated conformational changes, and their link with formation of the transient ammonia tunnel. We show that ammonia passage in PurL is controlled by two gates “mouth-gate” and “end-gate”, with the seed of the allosteric cycle residing at the “end-gate”. It was established that substrate entry at the formylglycinamide ribonucleotide (FGAM) synthetase domain both initiates end-gate opening and triggers conformational changes in the catalytic loop, which then passes the signal to the glutaminase domain. Molecular dynamics simulations indicate that during the catalytic cycle, the transient tunnel vacillates between open and partially closed states, which gives rise to a breathing ammonia channel that likely acts as a selectivity filter, which occludes solvent and provides directionality for ammonia passage. The mouth-gate network observed here was found to be a conserved feature in class 1 amidotransferases, hinting that a common mode of ammonia control exists across these enzymes.

KEYWORDS: *allosteric signal transduction, gating mechanism, purine biosynthesis, glutamine amidotransferase, formylglycinamide synthetase, pulsating ammonia tunnel*



INTRODUCTION

Tunnels in biological systems serve as conduits that allow controlled passage of molecules and act as selectivity filters as well as modulators of the catalytic efficiency to achieve precision in a chemical reaction.¹ For a subset of enzymes where the reaction intermediates are too reactive or toxic, evolution has created systems wherein fusion of two or more genes, originally encoding for independent proteins, functions as a coupled unit.² This physical association substantially enhances the rates of sequential reactions that they catalyze.³ In these systems, to coordinate the bifunctional reaction cascade, a fine-tuned signal transduction relay, that is intertwined via allostery, governs alteration in the population of catalytically competent states.^{4–7} Glutamine amidotransferases (GATs) serve as a classic example of enzymes that fall under this category. They exist as coupled bifunctional systems that transport ammonia to adjacent enzymatic units.⁸ These GATs via formation of internal tunnels provide reactive nitrogen to various metabolites for the survival of all living organisms.^{8–10}

In several instances, protein tunnels, generally ~25–100 Å in length,^{6,7} further fine-control the passage of intermediates via specific residues termed as “gates.” Gates are present either at the entry or exit or at the middle region of the tunnel and act

as internal allosteric bottlenecks for selective passage of a substrate.¹¹ Since these gating residues are not directly involved in the reaction cycle,^{11,12} they are sometimes not as harshly subject to the evolutionary rigor as required to preserve the fidelity of chemical reactions and can be variable across species. There are several kinds of gating architectures that have evolved in nature. The simplest of these are the wing-type gates that harbor a single bulky aromatic residue (phenylalanine, histidine, tyrosine, and tryptophan) at bottlenecks of the tunnels as in cytidine triphosphate synthetase (CTP)¹³ and imidazole glycerol phosphate synthase (IGPS)¹⁴ that swing in and out via a small angle rotation of the side chains. In addition, gates that involve a network of residues like the swinging door-type and aperture-type gates are also observed in several enzymes such as anthranilate synthase (AS) and carbamoyl phosphate synthetase (CPS).¹⁵ Being dynamic in nature, gates switch between “open” and “closed” conforma-

Received: December 1, 2021

Revised: January 7, 2022

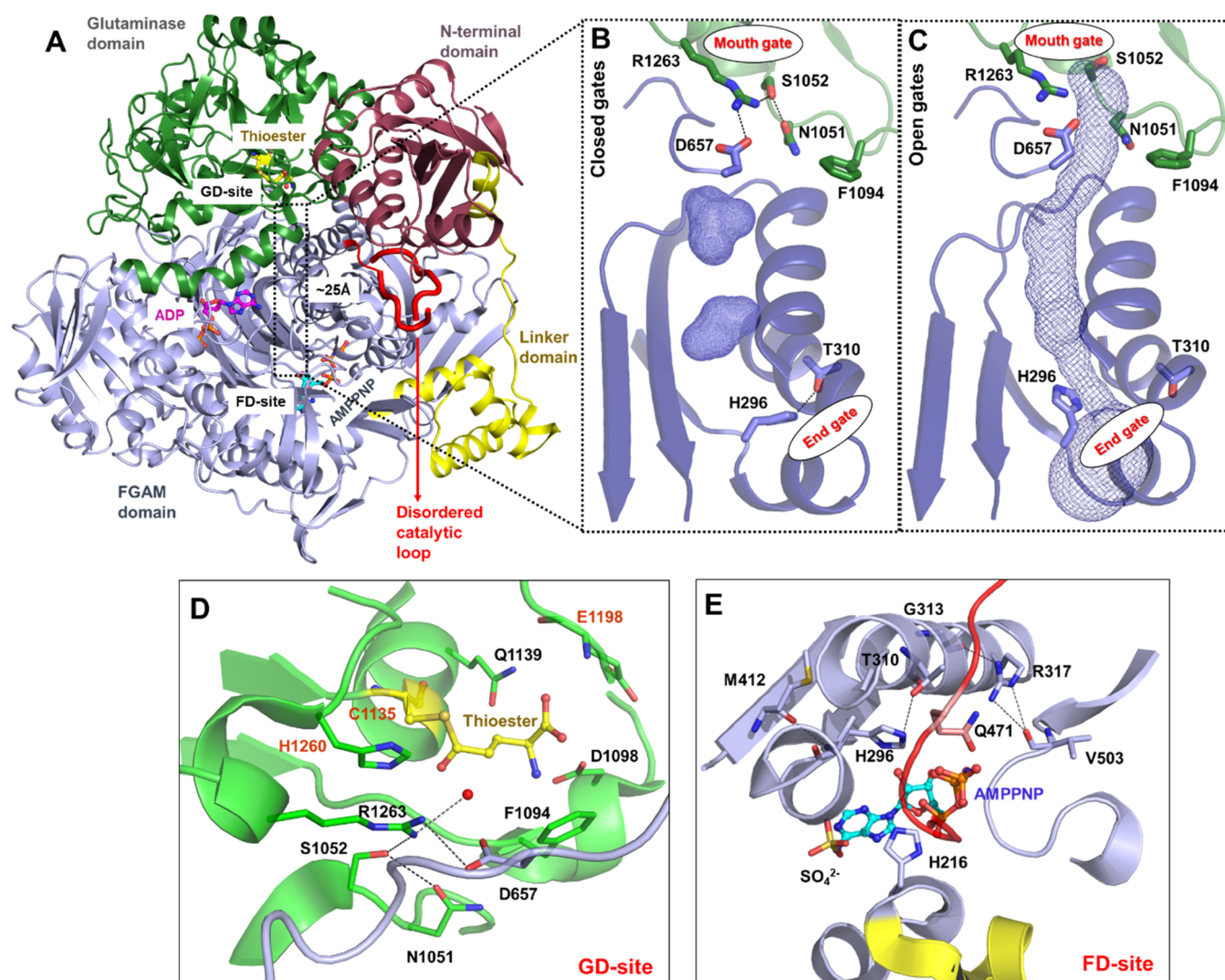
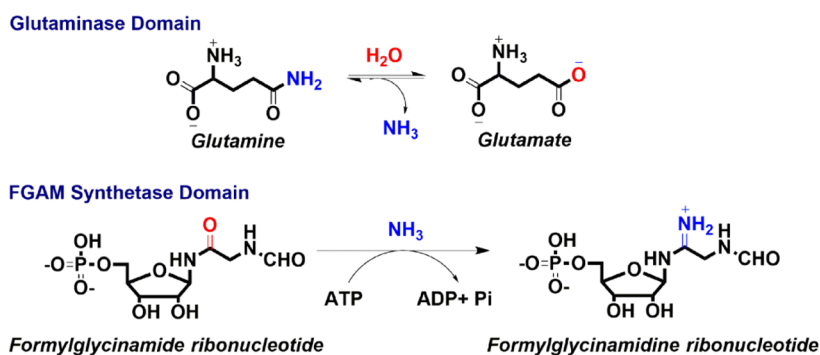


Figure 1. Overview of the native PurL crystal structure and ammonia channel connecting the two catalytic sites. (A) Crystal structure of the native PurL enzyme (PDB-ID 1T3T): N-terminal domain (NTD, salmon), linker domain (yellow), FGAM synthetase domain (FD, light blue), glutaminase domain (GD, green), catalytic loop (C-loop, red). Zoomed views showing (B) the native state of PurL with the closed gates (PDB-ID 1T3T) and disrupted ammonia channel and (C) the MD snapshot depicting the state where both gates are open at the two extreme ends to form the transient ammonia channel (blue mesh) using CAVER. The interaction network of the regions near (D) the mouth-gate below the GD-site where ammonia is produced and (E) the end-gate above the FD-site where ammonia is consumed. The red sphere in (D) represents a water molecule just below the thioester intermediate, most probably representing the position of just released ammonia after intermediate formation. Carbon atoms of the thioester intermediate, AMPPNP, and ADP are represented in yellow, cyan, and magenta in ball-and stick views, respectively. Oxygen and nitrogen atoms are depicted in red and blue. All figures are prepared in PyMol.

Scheme 1. Reaction Catalyzed by Formylglycinamide Synthetase



tions in a timely fashion^{1,11} and synchronize the catalytic events at the distal reaction centers.

To bridge the gap between the roles of gating residues in allosteric signal transduction and in correlating these events

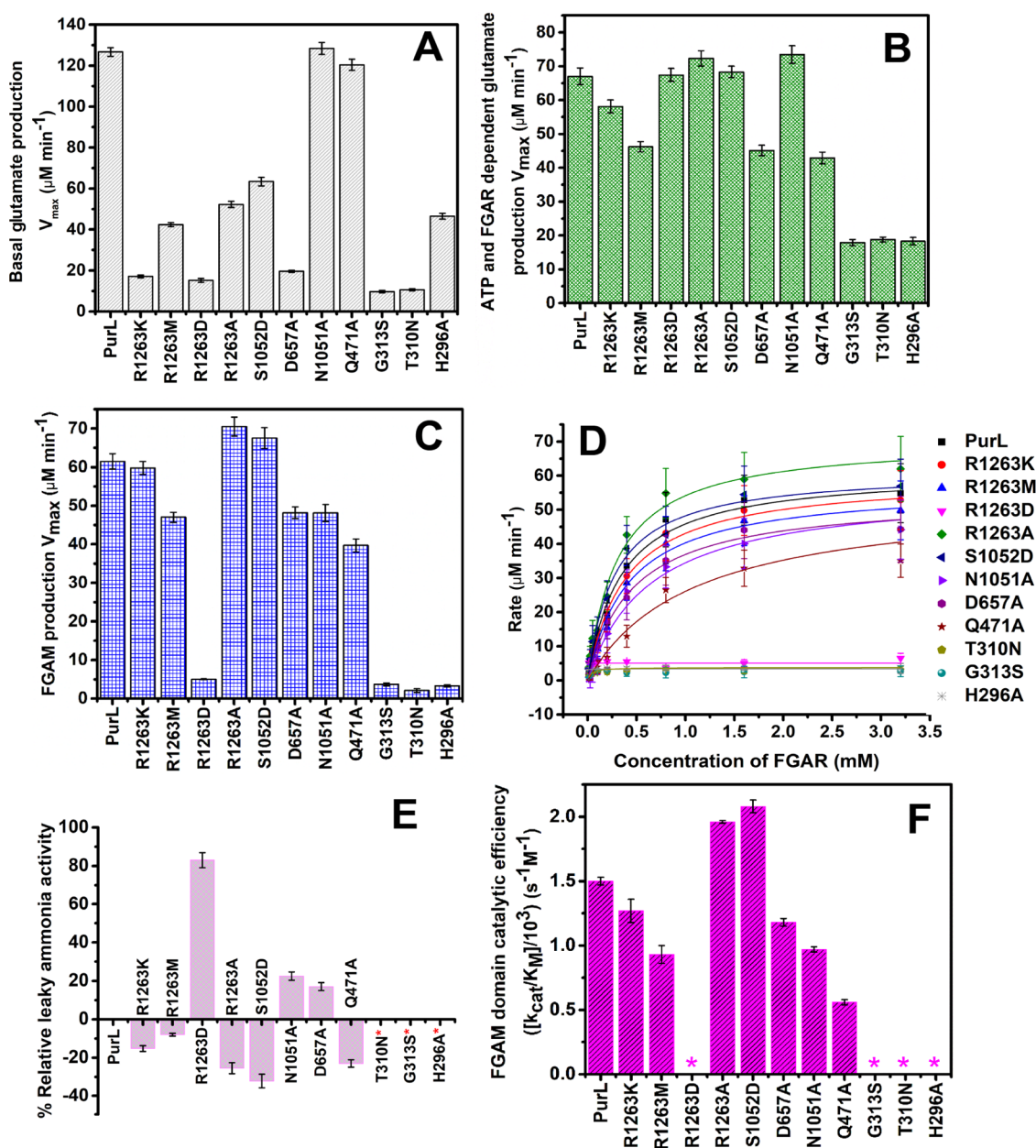


Figure 2. Activity profile of various PurL mutants at the mouth-gate and end-gate regions and the C-loop. V_{max} for the (A) basal glutamate production (gray bars), (B) ATP- and FGAR-dependent glutamate production (green bars), and (C) FGAM production (blue bars) of various PurL mutants. (D) Kinetic profile of the FD-site activity. The data is fitted in the Michaelis–Menten (MM) equation. (E) Relative leaky ammonia activity of the GD-site. (Red asterisk) indicates no leaky ammonia activity in the mutants due to no glutamate production. Columns and error bars represent the mean and standard deviation (SD) of three independent sets of reactions, respectively. The columns at the positive and negative axes represent the more and less leaky ammonia activity of the mutants compared to PurL, respectively. (F) Catalytic efficiency of the FD-site. (Purple asterisk) indicates the not-determined catalytic efficiency. The enzyme concentrations of all of the mutants and wild-type were kept the same for all of the data depicted.

with transient tunnel formation, we have selected formylglycinamide synthetase (PurL) from *Salmonella typhimurium* as a model for the present study. PurL is a bifunctional enzyme that catalyzes the fourth step in the purine biosynthetic pathway by converting formylglycinamide ribonucleotide (FGAR) to formylglycinamide ribonucleotide (FGAM) in an adenosine triphosphate (ATP)- and ammonia-dependent fashion in its FGAM synthetase domain (FD), which is also characterized to have an auxiliary adenosine diphosphate (ADP)-binding site whose function remains elusive (Figure 1A).^{16,17} Ammonia is produced via hydrolysis of glutamine in

its glutaminase domain (GD) and reaches the second reaction centre ~ 25 Å away in FD via formation of a transient tunnel (Scheme 1 and Figure 1A).^{16,18–20} The presence of an internal pathway sequesters ammonia from the bulk solvent, forestalls its entrance to the competitive metabolic pathways, and maintains its nucleophilic character.^{8,9,21–23} Although the structure of PurL was solved by Stubbe et al. in 2004,¹⁶ the identity of the tunnel and the signal transduction pathway remained elusive for over a decade. Recently, in 2020, using a combination of molecular dynamics (MD) simulations and biochemical studies, we were able to show a conserved

Table 1. Steady-State Kinetic Parameters of Various PurL Mutants

region of mutation	protein	V_{\max} ($\mu\text{M min}^{-1}$)	k_{cat} (s^{-1})	K_M or $K_{0.5}$ (mM)	$[k_{\text{cat}}/K_M]/10^3$ or $[k_{\text{cat}}/K_{0.5}]/10^3$ ($\text{s}^{-1} \text{M}^{-1}$)
Basal Glutamate Production ^a					
	PurL	126.7 ± 2.10	1.05 ± 0.07	3.20 ± 0.08	0.33 ± 0.017
mouth-gate	R1263K	17.1 ± 0.75	0.14 ± 0.002	3.50 ± 0.04	0.04 ± 0.002
mouth-gate	R1263M	42.4 ± 1.31	0.35 ± 0.05	22.60 ± 0.11	0.01 ± 0.001
mouth-gate	R1263D	15.2 ± 0.97	0.13 ± 0.07	13.89 ± 0.06	<0.01
mouth-gate	R1263A	52.3 ± 1.58	0.43 ± 0.03	2.33 ± 0.01	0.19 ± 0.011
mouth-gate	S1052D	63.4 ± 2.10	0.52 ± 0.04	1.75 ± 0.01	0.30 ± 0.022
mouth-gate	D657A	19.6 ± 0.50	0.16 ± 0.03	15.57 ± 0.09	<0.01
mouth-gate	N1051A	128.4 ± 2.97	1.07 ± 0.08	12.23 ± 0.05	0.09 ± 0.008
C-loop	Q471A	120.4 ± 2.70	1.00 ± 0.06	3.38 ± 0.04	0.29 ± 0.038
end-gate	G313S	9.7 ± 0.61	0.080 ± 0.004	ND ^b	
end-gate	T310N	10.6 ± 0.50	0.088 ± 0.003	ND	
end-gate	H296A	46.5 ± 1.41	0.39 ± 0.05	3.23 ± 0.03	0.12 ± 0.009
ATP- and FGAR-Dependent Glutamate Production ^c					
	PurL	67.0 ± 2.51	0.55 ± 0.02	1.36 ± 0.24 ($n = 0.53 \pm 0.05$)	0.41 ± 0.04
mouth-gate	R1263K	58.1 ± 1.92	0.48 ± 0.03	1.26 ± 0.02	0.38 ± 0.07
mouth-gate	R1263M	46.2 ± 1.55	0.38 ± 0.05	0.48 ± 0.05	0.80 ± 0.09
mouth-gate	R1263D	67.4 ± 1.90	0.55 ± 0.07	4.44 ± 0.16	0.13 ± 0.01
mouth-gate	R1263A	72.5 ± 2.38	0.60 ± 0.03	1.43 ± 0.08	0.42 ± 0.02
mouth-gate	S1052D	68.3 ± 1.79	0.57 ± 0.08	1.77 ± 0.13	0.32 ± 0.01
mouth-gate	D657A	45.1 ± 1.53	0.37 ± 0.02	6.27 ± 0.17	0.05 ± 0.03
mouth-gate	N1051A	73.5 ± 2.65	0.61 ± 0.05	1.63 ± 0.15 ($n = 0.48 \pm 0.08$)	0.37 ± 0.08
C-loop	Q471A	42.9 ± 1.76	0.35 ± 0.04	6.21 ± 0.11 ($n = 0.40 \pm 0.07$)	0.05 ± 0.01
end-gate	G313S	17.9 ± 0.72	0.15 ± 0.01	ND	
end-gate	T310N	18.8 ± 0.71	0.16 ± 0.03	ND	
end-gate	H296A	18.3 ± 1.14	0.15 ± 0.05	ND	
FGAM Production ^d					
	PurL	61.5 ± 2.15	0.51 ± 0.05	0.34 ± 0.05	1.50 ± 0.03
mouth-gate	R1263K	59.8 ± 1.16	0.49 ± 0.03	0.39 ± 0.03	1.27 ± 0.09
mouth-gate	R1263M	47.0 ± 1.34	0.39 ± 0.06	0.42 ± 0.07	0.93 ± 0.07
mouth-gate	R1263D	5.0 ± 0.10	0.04 ± 0.001	ND	
mouth-gate	R1263A	70.5 ± 2.50	0.59 ± 0.03	0.30 ± 0.05	1.96 ± 0.01
mouth-gate	S1052D	67.5 ± 2.71	0.56 ± 0.08	0.27 ± 0.04	2.08 ± 0.05
mouth-gate	D657A	48.2 ± 1.52	0.40 ± 0.03	0.34 ± 0.03	1.18 ± 0.03
mouth-gate	N1051A	48.1 ± 2.24	0.40 ± 0.06	0.41 ± 0.07	0.97 ± 0.02
C-loop	Q471A	39.7 ± 1.77	0.33 ± 0.04	0.59 ± 0.07	0.56 ± 0.02
end-gate	G313S	3.7 ± 0.41	0.030 ± 0.001	ND	
end-gate	T310N	2.1 ± 0.52	0.017 ± 0.005	ND	
end-gate	H296A	3.3 ± 0.30	0.027 ± 0.007	ND	

^aBasal glutamate production was monitored in the absence of ATP and FGAR. (Glutamate production was observed to be unaffected in the presence of ATP only.) ^bND, not determined. ^cGlutamate production was monitored using 10 mM ATP and 1 mM FGAR and at varying concentrations of L-glutamine. ^dFGAM production was monitored using 10 mM ATP and 50 mM L-glutamine and at varying concentrations of FGAR. Kinetic data was fitted in the Michaelis–Menten (MM) equation. In the case where substrate inhibition was observed, the data was fitted in the Hills equation. In these cases, the K_M value is $K_{0.5}$ and the obtained Hill coefficient (n) is given. k_{cat} , K_M , or $K_{0.5}$ and n values are the mean ± standard deviation (SD) of three independent sets of reactions.

catalytic loop (C-loop) that interacts with the substrate FGAR at the FGAM synthetase site (FD-site) to play a significant role in regulating the overall catalysis in PurL.²⁴ Along with stabilizing the substrate FGAR,¹⁸ the C-loop institutes long-distance communication with the glutaminase site (GD-site) via an adaptor N-terminal domain (NTD) (Video v1 and Figure S1A,B).²⁴ It was established that during the reaction cycle, the C-loop shuffles between the closed and open conformations and it is the partially open conformation of the C-loop where it forms a dynamic interface with NTD that serves as a key step in facilitating signal transduction (Figure S1A,B). Disruption of the dynamic C-loop/NTD interface was shown to abrogate both the distal glutaminase activity and the FGAM synthetase activity.²⁴ MD analysis shows that coordinated motion in the C-loop aids both glutamine

hydrolysis and in the formation of a hydrophobic transient ammonia tunnel (Video v2), thereby connecting the two catalytic sites.²⁴ Two gates (Figure 1B,C), one at the start of the tunnel “mouth” and the other at its bottom “end”, were proposed to control the passage of ammonia.²⁴ Although this initial work was seminal in providing several clues that helped to propose a signaling cascade, several important gaps remained unanswered. Details as to how these two gates open and close and how the transient ammonia tunnel formation is facilitated as well as the complete molecular details connecting the entire catalytic cycle remain elusive.

In the present work, to develop a comprehensive connection between the signaling, tunneling, and catalytic cycle, we performed a combination of mutagenesis, biochemical, and X-ray crystallographic studies along with MD analysis. We

delineated the importance of the gating network (Figure 1D,E) and the precise order of gating as well as the seed of the allosteric control was established. Moreover, MD simulations lead us to an important phenomenon of a pulsating ammonia tunnel. It was observed that instead of a tunnel that is either fully open or closed during the catalytic cycle, the transient tunnel vacillates between partially closed (pC-state) and fully open (O state) states before it closes. Overall, the results from this study provide a broad understanding of how systems that transfer reactive intermediates fine-control their passage and additionally hint at the possibility that a pulsating tunnel may be a widespread phenomenon in nature, a hypothesis that needs to be experimentally validated.

RESULTS

Ammonia Regulation at Mouth-Gate. PurL belongs to class-I amidotransferase superfamily that harbors a catalytic triad comprising cysteine, histidine, and glutamate residues, paramount for activity (Figure 1D).^{8,16} It also harbors an oxyanion loop that contains a conserved GG motif, which constitutes the oxyanion hole residues, proposed to help in stabilization of the anionic transition state.¹⁶ Analysis of PurL sequences reveals that the residues at the periphery of the GD-site that are not directly involved in catalysis are 100% conserved (analyzed for 1000 PurL sequences using the ConSurf online server²⁵) (Figure S2). Inspection of the thioester-bound form of native PurL (PDB-ID 1T3T) shows that R1263 forms a connected network and interacts with a water molecule that is situated at the same place where ammonia is expected to be released (Figure 1D and Video v3). It also forms a salt bridge with an interfacial residue D657 (present in a loop between helix α 18 and strand β 25 in the FD) (Figure 1D and Video v3). R1263 is additionally hydrogen-bonded to S1052, which lies opposite to it. S1052 in turn interacts with the neighboring N1051 that is hydrogen-bonded to the GG oxyanion motif and also interacts with the FD residues (Figure 1D and Video v3). Both D657 and N1051 are situated on opposite sides of the wall of the tunnel and contact the central tunnel-lining residues (Figure S3A). Thus, four peripheral residues R1263, S1052, D657, and N1051 form a defined hydrogen-bonding network, which is proposed to serve as a “mouth-gate” (Video v3).

To understand the role these gating residues play in regulating catalysis and in crosstalk between the active sites, systematic mutations of this region were performed. In particular, to investigate whether the positively charged residue R1263 plays a role in controlling ammonia release, it was systematically mutated to another positively charged, acidic, hydrophobic, as well as small residue alanine. Corroborating mutations of the other residues in the interacting sphere such as S1052, D657, and N1051 were also constructed, and the secondary structures of the proteins expressed were confirmed via CD (Figure S3B). Subsequently, a detailed kinetic analysis of the native and mutants was performed for three different activities: basal activity of GD, that is, ammonia production in the absence of the FD-site substrates ATP and FGAR, ammonia production in the presence of ATP and FGAR, and the FGAM synthetase activity in the presence of all three substrates (Figures 2 and S4 and Table 1). It was observed that *S. typhimurium* PurL has a very high level of basal activity in the absence of FGAR (Figures 2A and S4A and Table 1). Stubbe and co-workers have also reported that *Escherichia coli* FGAM synthetase, another Gram-positive eubacteria, which

exhibits 93% sequence similarity to PurL, also exhibits a similar basal profile.²⁶ On the contrary, *Bacillus subtilis* PurQ is unable to catalyze glutamine hydrolysis efficiently by itself.²⁷ Addition of ATP and FGAR resulted in a decrease in $k_{\text{cat}} (V_{\text{max}})$ by half of the basal value for the native PurL (Figures 2B and S4B and Table 1), and a comparison of $k_{\text{cat}} (V_{\text{max}})$ of the native FD-site activity with that of the glutaminase activity shows that both $k_{\text{cat}} (V_{\text{max}})$ values are comparable (Figures 2B–D and S4B and Table 1). Thus, ATP and FGAR both tune the reactivity at the GD-site such that both rates are optimized to match the FD-site reaction. It was noticed that the basal activity is dramatically affected when R1263 is changed to any other residues (Figure 2A and S4A and Table 1). While the basal activity of R1263M has a $k_{\text{cat}} (V_{\text{max}})$ that is reduced threefold, R1263A shows a twofold reduction (Figures 2A and S4A and Table 1). Introduction of charged amino acids such as mutations R1263K and R1263D results in a sharp decrease in basal activity (Figures 2A and S4A and Table 1).

Surprisingly, the profile shows a dramatic shift upon the addition of ATP and FGAR. Several mutants that showed minimal basal signal regain their GD activity (Figures 2B and S4B and Table 1). Mutants R1263A and R1263D behave like the native and exhibit ammonia production similar to that of native PurL in the presence of ATP and FGAR (Figures 2B and S4B and Table 1). However, R1263M shows a decrease of 35% and R1263A shows an opposite effect of enhancement of the activity by 10% with respect to the native under similar conditions (Figures 2B and S4B and Table 1). What is most intriguing is that R1263A has a much lower basal activity, but after stimulation by ATP and FGAR, the pattern has reversed (Figures 2A,B and S4A,B and Table 1), which highlights that the FD-site substrates have a profound effect on the GD-site activity. Even more interesting is the trend in the FGAM synthetase activity. While R1263K behaves like the native as expected because of the replacement of an analogous positive charge, R1263M has around 25% reduction (Figure 2C,D and Table 1). The most dramatic loss of activity is for R1263D. This mutant shows good ammonia production in the presence of FGAR but has 90% reduced FGAM synthetase activity (Figures 2B–D and S4B and Table 1), most likely because not only in this case the D657–R1263 salt bridge is disrupted but also the juxtaposition of two negative charges causes repulsion, leading to misorientation of D657. On the contrary, R1263A has both enhanced ammonia production and a 15% increase in the FGAM synthetase activity (Figures 2B–D and S4B and Table 1) and seems to be the most favorable mutant with respect to enzyme performance as it is also less leaky than the native PurL (Figure 2E). Another peripheral mutation that mimics the R1263A activity profile is S1052D. This mutant also shows slightly enhanced ammonia production and FGAM synthetase activity (9–10%) (Figures 2B–D and S4B and Table 1) with lower overall leakage of ammonia (Figure 2E).

The kinetics of mutants D657A and N1051A that bridge the tunnel-lining residues with the mouth-gate hydrogen-bonding network (Figure S3A) were also analyzed. Here, it was observed that N1051A shows a similar basal ammonia activity profile to the native and a slight 9% enhanced glutaminase activity with respect to the native in the presence of ATP and FGAR (Figures 2A,B and S4A,B and Table 1). However, D657A has a significantly stunted basal activity, which is stimulated somewhat in the presence of ATP and FGAR but is still 31% lower than the native (Figures 2A,B and S4A,B and Table 1). As a result, D657A also has 25% reduced FGAM

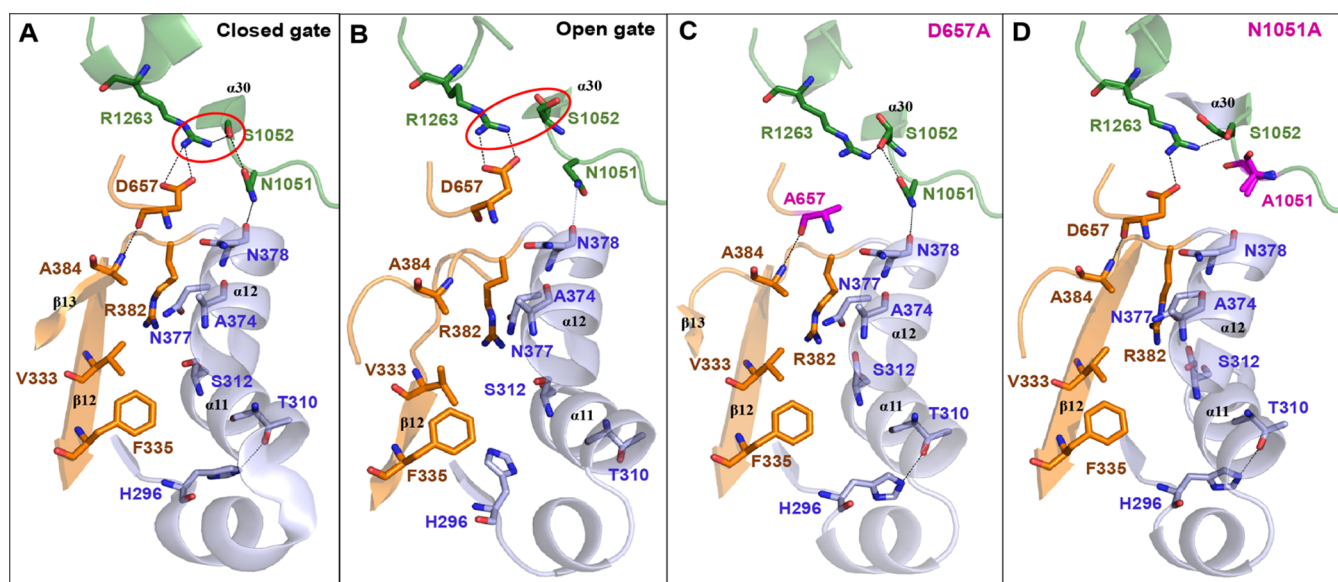


Figure 3. Role of D657 and N1051 residues in signal transmission and ammonia channel formation. The hydrogen-bonding network of the mouth-gate region near the G-site and channel-lining residues of the crystal structures of mutants R1263A, R657A, and N1051A (determined in this study) and the native and MD snapshots are compared. (A) Native PurL (PDB-ID 1T3T) showing the closed-gate conformation and (B) 570 ns MD snapshot depicting the open-gate conformation wherein the R1263–D657 salt bridge swings out away from the G-site, resulting in disruption of the D657 interaction with the A384 residue, opening the channel. Mouth-gate swinging motion for gate opening is highlighted in the red dotted circle. In (C) D657A and (D) N1051A mutants, the hydrogen-bonding interactions between R1263–A657 and A1051–N378 are disrupted respectively; however, backbone interaction of residues 384 and 657 is maintained, resulting in improper channel opening. Residues from GD and FD are shown in green and blue sticks, respectively, while the mutated residues are shown in magenta sticks. Regions showing substantial conformational changes during channel formation are highlighted in orange.

synthetase activity (Figure 2C,D and Table 1). Surprisingly, although N1051A is an efficient ammonia producer, most of its ammonia leaks (Figure 2E) and it still exhibits 25% reduced FGAM synthetase activity (Figure 2C,D and Table 1). Thus, mutation of both D657 and N1051, the tunnel-lining residues, which are more than 20 Å away from the FD-site, leads to the loss of FGAM production.

Overall, the activity assay data shows that although R1263 is not a core catalytic residue, it does partake in imparting higher catalytic efficiency to the GD-site as the basal activity of the native enzyme is maximal and this activity is markedly affected when it is replaced by any other residue (Figures 2A and S4A and Table 1). Moreover, R1263A and S1052D both have enhanced ammonia and FGAM production and are slightly catalytically more efficient than the native (Figures 2B–F and S4B and Table 1). Although mutations at these positions are tolerated, any mutation that clashes with the conserved D657 significantly stunts the FGAM synthetase activity.

Signal Relay via the Mouth-Gate. To understand the activity assay results more clearly, a series of crystal structures for R1263A, D657A, S1052D, and N1051A were solved (Table S1). All of the mutants for which crystal structures were determined were found to be isomorphous to the wild type. Based on the examination of the crystal structures of the various mouth-gate mutants and the MD snapshots (Figures 3A–D and S5A–D), the mechanism of tunnel opening with respect to the four gating residues was analyzed. The role of R1263 and S1052 was attributed primarily to the opening and closing of the mouth-gate (Figure 1B,C). It was noticed that in the closed-gate conformation (Figure 3A), R1263 and S1052 form a hydrogen bond, whereas in the open conformation (Figure 3B), R1263 swings out along with D657 via salt bridge formation, and concomitantly, S1052 also flips away from the

exit path of ammonia, breaking its hydrogen-bonding interaction with N1051. Thus, the interaction of R1263 with S1052 and D657 keeps the gate closed (Figure S5A). In the absence of arginine at 1263, the high-resolution crystal structure reveals that the previously interacting residues S1052 and D657 adopt alternate conformations in the crystal structure (Figure S5B), indicative of a high degree of flexibility, implicating that the gating controls are now compromised as neither S1052 is hydrogen-bonded nor D657. Also, in the absence of this R1263 residue, ammonia is likely free to flow into the tunnel, which explains the increase in activity and lower leakage profile (Figure S5B). A similar scenario is observed for the S1052D mutant, where from the crystal structure it is evident that aspartate at this position points away from R1263 and is no longer hydrogen-bonded to it (Figure S5C). Thus, when the gating control is compromised, a rapid escape of ammonia directly into the channel occurs as is corroborated by the enhanced activity at both the reaction centers (Figure 2B–D and Table 1).

The crystal structure of the native PurL (PDB-ID 1T3T) shows that in the native protein, D657 hydrogen-bonds with both R1263 and tunnel wall residue A384 (Figure 3A), which lies on strand β 13. Earlier insights from MD into the native PurL system, where the tunnel opening and closing events were visualized, additionally revealed that, in the channel open state, this region undergoes significant conformational changes, which induce formation of the transient tunnel (Figure 3A,B).²⁴ Here, the snapshots showed that the distance between the backbones of D657 and A384 increases (Figure 3B), and overall, signaling between D657 and A384 is one of the factors that coordinates tunnel opening. The crystal structure of the D657A mutant corroborates the observations from the MD snapshots (Figure 3B,C). The structure shows that the salt

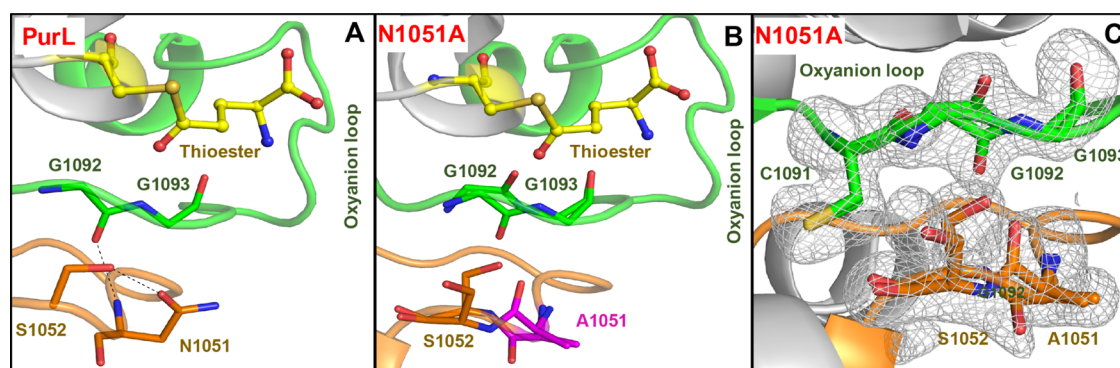


Figure 4. Signal transmission to the oxyanion loop via the mouth-gate network leads to activation of ammonia production. Crystal structures showing the hydrogen-bonding network at the oxyanion hole and mouth-gate region of the GD-site in (A) native PurL and (B) N1051A mutant. The mutated residue is represented by a magenta stick, and the thioester intermediate is modeled using the native PurL structure (PDB-ID 1T3T). Residues are shown in stick view. (C) Electron density map contoured at 2.0σ using the mFo-DFc map depicting the active and inactive conformations of the oxyanion loop (green) and assisting loop (orange). In (B) and (C), both the active and inactive conformations of the oxyanion are captured and the loop assisting these conformations (orange) also adopts an alternate conformation.

bridge interaction that was mediated by the carboxylic head group with R1263 is lost in the D657A mutant (Figures 3A,B and SSD) and the alanine introduced at position 657 results in a shift of this residue toward A384 via backbone hydrogen-bonding interactions (Figure 3C). The disruption of R1263–D657 interaction in this mutant promotes tighter interaction between backbones of the residues at 384 and 657 positions (Figure 3C), thereby precluding proper tunnel opening/closing. Further analysis of the crystal structure of interfacial D657A revealed that this mutation, which is situated near the GD-site, results in changes in the structure ~ 25 Å away at the FD-site (Figure S6). Overall, disordering of the catalytic FD-site is observed with residue H216 and the previously ordered water molecule network present in the native enzyme crystal structure around this region becomes diffuse (Figure S6). To confirm that this is a real observation, Fo-Fc and 2Fo-Fc maps used to compare water networks were constructed within the same resolution limits. The result indicates that in D657A, the FD-site is more solvent-exposed (Figure S6). The catalytic efficiency of D657A is significantly reduced both in terms of ATP- and FGAR-stimulated ammonia production and FGAM synthetase activity (Figure 2B,C). Therefore, it is possible that D657, which serves as a bridge between GD and FD, is a crucial modulator for the FGAM synthetase activity. It is via dual hydrogen-bonding interaction with R1263 and A384 that it appears to play a central role in signaling the gate opening event that facilitates formation of the transient ammonia tunnel and downstream ordering of the FD-site. An analogous residue to D657 is found at this interfacial position in almost all class-I GATs. It has been also demonstrated in other systems that mutating this residue in AS, IGPS, 2-amino-2-deoxyisochorismate synthase (PhzE), and 4-amino-4-deoxychorismate synthase (ADCS) resulted in impaired allosteric coupling in glutaminase and synthetase subunits.²⁸ In PurL also, this conserved aspartate residue serves the same purpose, thereby highlighting that GATs have a common signal transduction pathway.

To get clues regarding the contradictory activity profile of N1051A, the crystal structure of N1051A was solved and compared to that of the native. In native PurL along with interaction with S1052, the amide group of the N1051 residue interacts with the backbone carbonyl of G1092 (a conserved oxyanion strand residue in all GATs) (Figure 4A). MD studies

showed that during transient ammonia channel formation, N1051 changes its conformation and releases the oxyanion loop, allowing it to undergo rearrangements for stabilizing the transition state by flipping G1092 into the GD-site (Figure S7). In the high-resolution X-ray structure of the N1051A mutant, G1092 is observed in a dual conformation: both flipped-in and flipped-out (Figure 4B,C). Trapping the oxyanion loop in a productive conformation has been experimentally challenging. A similar type of flipping was predicted via MD simulations for the IGPS system and proposed to be a conformation that stabilizes the anionic tetrahedral transition state during glutamine hydrolysis (Scheme S1).²⁹ It appears that the flexibility induced in the oxyanion loop due to the loss of anchoring via the asparagine side chain in N1051A makes the oxyanion loop more mobile (Figure 4B,C) and results in ease of attaining a conducive transition state, leading to enhanced ammonia production (Figure 2B). N1051 is also a bridging residue that communicates the progress of the reaction to the tunnel via hydrogen bonding to N378 that lies on $\alpha 12$, a helix that shows significant rearrangement upon tunnel formation as observed by MD (Figure 3A,B). In N1051A, the interaction of N378 is disrupted (Figure 3D); therefore, accurate information from this side of the tunnel wall regarding the progress of ammonia production does not reach N378 and, in turn, the downstream residues. Besides, the N1051A mutant enhances the glutamine hydrolysis potential (Figure 2B), but the FGAM synthetase profiles show a reduction in FGAM production (Figure 2C). A similar scenario of impaired signaling is observed for the other tunnel communicating residue D657, reasserting that both these residues, which line the opposite ends of the tunnel mouth, pass the signal via restructuring the tunnel-lining residues and enable formation of the transient ammonia tunnel.

Role of End-Gate Residues in Signal Transmission.

The end-gate (H296–T310) is present in the FD of PurL on helix $\alpha 11$ (Figure 1E), just above the FGAR- and ATP-binding site that bears the signature sequence (Dx₄/6GAXP) of the PurM/PurL family of ATP-binding proteins.^{16,19} In the native PurL structure (PDB-ID 1T3T), this gate is present in a closed conformation, where residue H296 is hydrogen-bonded with the hydroxyl group of T310, an opposite wall residue closing the exit path of ammonia (Figure 1B,E). MD simulation results

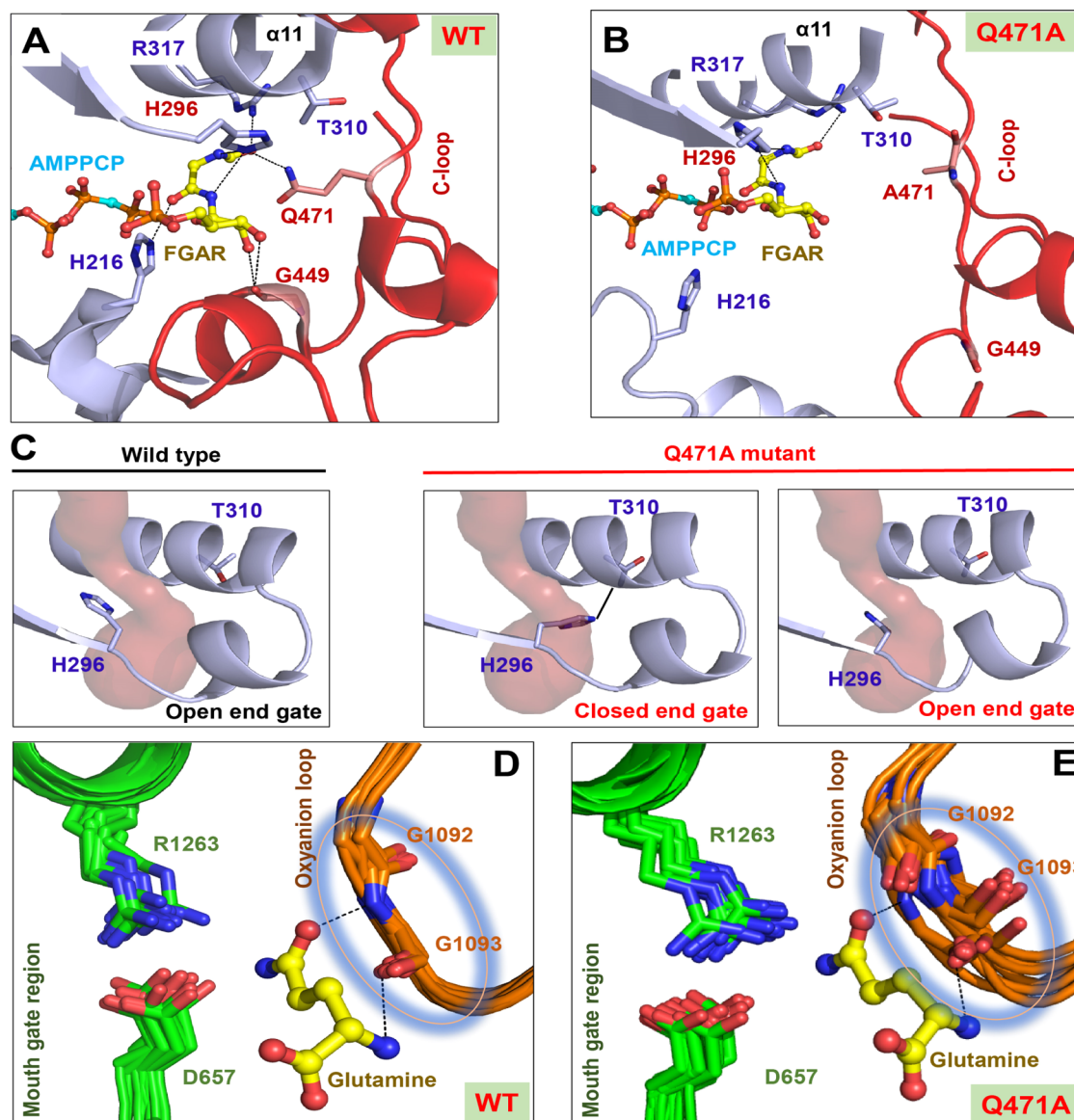


Figure 5. Signal transmission by the end-gate to the C-loop. (A) Substrate-bound state, as seen in the FGAR- and AMPPCP-bound TmPurL (PDB-ID 2HS4) crystal structure. In this state, the C-loop residue Q471 (salmon) helps H296 to adopt a conformation that stabilizes the formylglycinamide side chain of FGAR (yellow ball and stick), where the $-NH-$ of formylglycinamide side chain forms a hydrogen bond with H296. (B) Substrate-bound state mimicked in the MD snapshot of Q471A mutant probed in native PurL; the interaction between the C-loop and H296 residue is lost. The C-loop and FGAM domain are shown in red and light blue, respectively. AMPPCP and FGAR are shown in cyan and yellow ball-and-stick view. End-gate residues H296 and T310 adopted (C) an open conformation in native PurL, while both open and closed (via hydrogen-bonding interactions) conformations in the Q471A mutant over the simulation length. (D) Oxyanion loop (orange) in the mouth-gate region remains in a conformation favorable for stabilizing the transition state by forming hydrogen bonding with glutamine via the G1092 and G1093 residue backbone, indicating intact signal transmission to the GD-site. However, (E) these residues were observed to be adopting both favorable and unfavorable conformations in the Q471A mutant over the length of the simulation, indicating disrupted signaling toward the GD-site for ammonia production.

show that during the catalytic cycle, H296 swings away from the FD-site, which results in disruption of the H296–T310 hydrogen-bonding interaction, thereby opening this gate (Figure 1C).²⁴ Moreover, analysis of the MD snapshots reveals that the end-gate remains open during the entire catalytic cycle.²⁴ However, how this information gets transmitted to the FD-site and its implications on catalysis are not well understood.

In this context, H296 was mutated to alanine to achieve a permanent open-gate conformation. It is reported that H296 is also a catalytically important residue, whereas T310 does not

directly participate in catalysis. H296 has been shown to interact with FGAR and help in proton donation (Scheme S2).¹⁸ As expected, the FGAM synthetase activity of the H296A mutant is completely abrogated (Figures 2C and S4C and Table 1). It is however observed that this mutant was able to bind glutamine in the absence of FGAR (Figure S8 and Table S2) and also exhibited threefold reduced basal ammonia/glutaminase activity when compared to the native (Figures 2A and S4A and Table 1). However, in the presence of the substrate (FGAR and ATP), this basal activity was completely lost in H296A (Figures 2B,C and S4B,C and Table

1). Thus, corroborating that the communication to the GD-site is enabled via the interaction network that is formed upon binding of the substrate FGAR.

To create a scenario wherein the end-gate is potentially permanently closed, two mutations near H296, that strengthen the overall hydrogen bonding at the end-gate, were designed. The first mutation was replacement of T310 by an asparagine residue, and the second mutation was replacement of G313 by a hydrogen bond donor serine. While T310 directly hydrogen-bonds with H296, keeping the gate closed, G313 lies adjacent to the gate. The design rests on the premise that preserving H296 will not disturb the catalytic core, but these mutations will rather allow the gating contacts to be strengthened. CD results reveal that both these mutants fold properly (Figure S9) but exhibit absolutely no FGAM synthetase or glutaminase activity (Figures 2B,C and S4B,C and Table 1), and they also do not exhibit any basal ammonia activity (Figures 2A and S4A and Table 1). Thus, a complete shutdown of the system was surprising as neither T310 nor G313 are core catalytic residues and are not envisioned to play any role in catalysis. Conservation analysis shows that both these residues are 100% conserved in all IgPurLs (Figure S2). Supporting isothermal calorimetric (ITC) studies show that both T310N and G313S PurL mutants are additionally incapable of binding glutamine (Figure S8 and Table S2). These results indicate that in the closed-gate scenario, the GD-site, which is 25 Å away, is also inaccessible. This asserts that residues that are not directly involved in catalysis but play a role in keeping the gate integrity are equally important in maintaining the catalytic cycle. Complete abrogation of the glutaminase activity indicates that long-distance communication is at play and the initiating step in the signal transduction pathway is opening of the end-gate mediated by peripheral residues such as T310 and G313.

Role of C-Loop in Signal Transduction. Previous crystallographic and MD studies revealed that the C-loop dramatically changes its conformation during the course of the reaction and creates a dynamic interface with the NTD for allosteric signal transduction.²⁴ However, which step in catalysis triggers the C-loop movement was not clear. To delve deeper into this question, using the FGAR-bound TmPurL structure (PDB-ID: 2HS4)¹⁸ (Figure 5A and Video v4) and the MD snapshots of native PurL (Figure 5B), we created a model of the FGAR-bound state. It was observed in the precatalytic state that FGAR binding results in changes in the conformation of H296 (Figures 5A and S10A).

Structural comparison between apo (PDB-ID 1T3T) and FGAR-bound states (PDB-ID 2HS4) shows that Q471 moves inward to the substrate by ~2.7 Å with respect to its native conformation, thereby hydrogen-bonding with H296A (Figures 5A and S10A). Thus, to reiterate, in the precatalytic state before the reaction proceeds, H296 interacts with both T310 and Q471, keeping both the gate and C-loop anchored (Figure 5A). When the reaction proceeds, MD conformations show that in the open-gate conformation both H296–T310 and H296–Q471 interactions were missing and H296 had rotated away from the FD-site (Figures 5B and S10B). During the signal transduction event when H296 flips to open the gate, Q471 concomitantly moves away from H296, outward, where it is stabilized near the NTD–FD junction; thus, the allosteric cycle is initiated (Figure S10C,D).

To confirm the role of Q471, a mutant version of the enzyme, wherein this residue is mutated to alanine, was

constructed. The Q471A mutant resulted in more than 50% reduction in both glutaminase and FGAM synthetase catalytic efficiencies (Figures 2A–C and S4A–C and Table 1). Moreover, to understand the importance of Q471 in signaling, a 750 ns simulation of the Q471A mutant version of the protein was carried out. Analysis of the Q471A mutant by MD shows that the C-loop conformation is distorted 50% of the time in the trajectory (Figure 11A,B). Therefore, effective transfer of the signal from the C-loop to NTD does not occur half the time. In native PurL, MD shows that the end-gate (H296–T310) remains permanently open throughout the catalytic cycle,²⁴ while in the Q471A MD simulation, the end-gate is open 50% of the time and closed rest of the 50% (Figure 5C). Similarly, the restructuring of the oxyanion loop, which is important to attain for competent glutamine hydrolysis, is also only effectively positioned approximately 50% of the time (Figure 5D,E). This asserts that Q471 indeed plays an important role in crosstalk and the allosteric signal is ineffectively transferred if Q471 is unable to communicate with the gating residue H296.

Pulsating Ammonia Tunnel. The changes in catalytic rates of the mutants and crystallographic snapshots of the mutants motivated us to delve deeper into the events that influence transient tunnel formation. Analysis of the MD snapshots by the CAVER PyMoL plugin³⁰ over the length of the simulation clearly showed that the tunnel is not open completely through the catalytic cycle but rather vacillates between O and pC states with the opening and closing time varying over the simulation time scale (Figure 6). To better visualize the conformational changes that trigger the breathing motion between the O and pC states, the residue pair distances of the channel-lining residues were plotted over the simulation time scale (Figure 6). Distances and CAVER analyses showed that in addition to the open conformations adopted by both the gating residues, the bottleneck residues present below the mouth-gate at the start of the tunnel (N377, N378, R382, A384) play a crucial role in regulating access to the tunnel and forming an aperture (Figure 7). Over the open tunnel phase, the tunnel aperture vacillates between pC and O states where residues move in a correlated manner. The (distance) fluctuations in the signaling residues D657 and N1051 are transmitted to the neighboring N378, R382, and A384 residues (Figure 6). These residues move apart, resulting in opening of the tunnel for a period of 100–150 ns (O state; Figure S12A) while coming closer for 125–200 ns, disrupting access to the tunnel (pC-state; Figure S12B). In the completely closed state, these residues come even closer, thereby keeping the aperture tightly closed (Figure S12C). At instances where the tunnel is fully open and the mouth-gate R1263–S1052 pair is apart (6.8 Å), the swinging motion of the mouth-gate R1263 residue transmits the signal to the D657 interfacial residue, pulling it toward itself and disrupting the hydrogen bond between D657 and A384 (Figure 3B). In this state, the bottlenecks are removed and the central tunnel wall residue V333 moves such that it faces away from A384, thereby creating space (Figure 3B). The pulsating tunnel was an interesting observation and reminiscent of conformational selection adopted by enzymes, where it was noted in several examples that via breathing motions, sometimes assisted by ligands/substrates, an environment is created to attain selectivity of function.³¹

Further, to develop a comprehensive understanding of the signal transmission process, cross correlations for residues lining the tunnel, C-loop, mouth and end gates as well as the

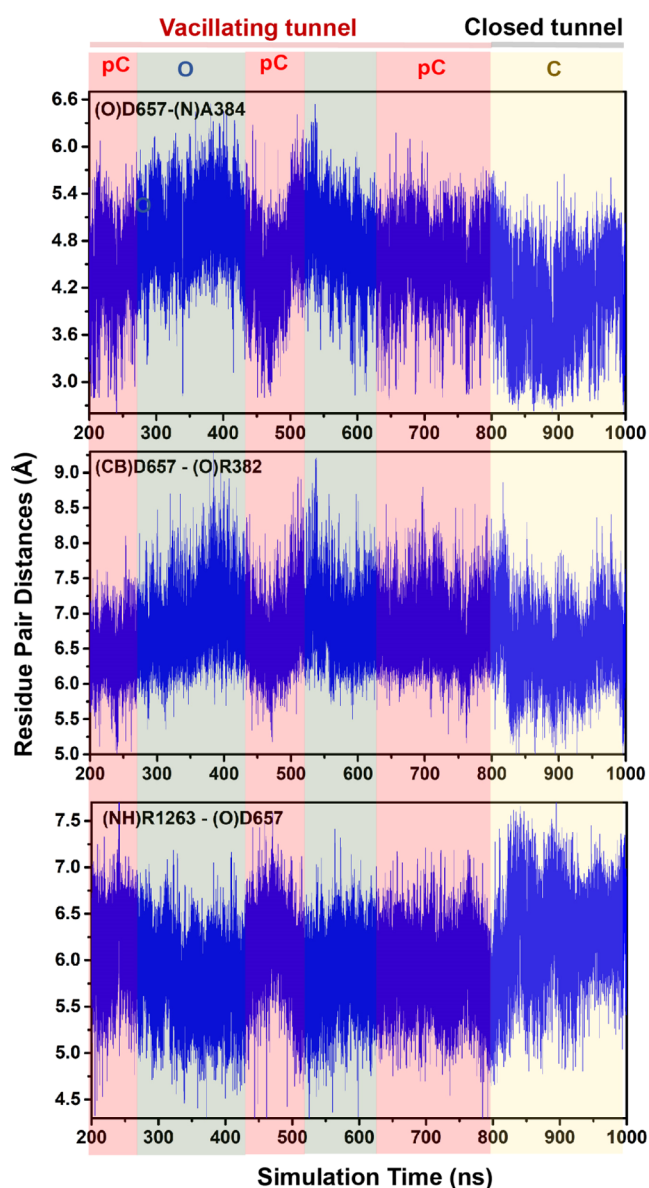


Figure 6. Correlated motion of the gating and channel-lining residues. Correlated motion of the mouth-gate and channel-lining residue pair distances over the length of the simulation, resulting in channel opening and partially closing via this synchronous motion. The time representing the partially closed tunnel state “pC” are highlighted in red shadow, the open (tunnel) state “O” are highlighted in blue shadow while that representing the completely closed “C-state” are shown in light yellow shadow.

dynamic NTD interface were plotted for both the open and closed time periods (Figure S12D,E). Analyses show that indeed in the open tunnel time period, strong correlations among residues that connect the mouth-gate with the tunnel-lining residues exist. Here, pairwise distance correlations show that in the tunnel open configuration, the D657–A384 distance is correlated with both the mouth-gate opening event and the downstream tunnel-lining residues (V333, S312, L332, N377, and R382) (Figure S12D). This residue pair is also very highly correlated with the end-gate (H296, Q471) as well as the dynamic NTD/C-loop region (R80–V470, F467 couples) (Figure S12D) and appears to be central to communication. Cross-correlation analysis also shows that in the tunnel closed state (801–1000 ns) (Figure S12E), subtle

shifts occur and the D657–A384 couple no longer shows correlation with the channel-lining residues or the mouth and end gates as well as the NTD interface, indicating collapsed communication. Thus, the transient tunnel opening event is not a static state; rather, the tunnel is a breathing entity that perhaps allows ammonia to squeeze through it. The pulsating tunnel as visualized in the PurL system could be a wider phenomenon and perhaps applicable to several systems wherein directionality of transfer is crucial. It may also help to keep water and other solvent molecules from accidentally entering the tunnel.

DISCUSSION

Mechanism of Control of Glutaminase Activity.

Ammonia channeling enzymes are examples of systems that have strongly coupled active centers and whose reactivity of the active sites is controlled in various diverse manners. In several instances, multiple checks and controls are kept to maintain the stringency of the system. The series of kinetic analyses, crystal structures, and simulation studies provide additional insights into the mechanism of crosstalk in FGAM synthetase as well as open several questions into the complex allosteric relay that controls the reactivity of this bifunctional enzyme. What is most notable is the regulation of the glutaminase activity by addition of ATP and FGAR. Surprisingly, the enzyme has a high level of basal activity, i.e., efficiently catalyzing glutamine in the absence of substrates in the adjacent FD-site (Figures 2A and S4A and Table 1). Interestingly, in the presence of ATP and FGAR, the glutaminase activity is tuned down to match the catalytic rate of the FGAM synthetase reaction (Figures 2B,C and S4B,C and Table 1). It is not exactly established how the presence of FGAR tunes the activity of GD. However, the experimental probing of the allosteric network as well as the MD points to a scenario wherein the entry of FGAR activates the allosteric pathway that controls the exit and entry of glutamine via the motion of the C-loop/NTD/GD interface, which in turn also influences the conformation of the oxyanion loop.²⁴ Mutation of Q471A experimentally partially confirms this hypothesis. The MD of Q471A mutant reveals that the disturbance in the C-loop network leads to substantially impaired signaling both via misregulation of the C-loop/NTD interface and distortion of the oxyanion hole (Figure 5). Previous reports also confirm that mutation of the C-loop/NTD interface leads to a complete loss of glutaminase activity as well as a loss of glutamine binding.²⁴

The study further highlights that end-gate is the most important control unit. It acts as a master switch and regulates the entire bifunctional system. Any perturbation of the end-gate network results in complete abrogation of both the FGAM synthetase and the distal glutaminase activity (Figures 2A–C and S4A–C and Table 1). Because purine biosynthesis is a central and important pathway for the synthesis of DNA/RNA precursors, it is possible that enzymes in this pathway have added checks and balances to ensure fidelity. A survey of a few other ammonia channeling enzymes revealed that guanosine monophosphate (GMP) and cytidine triphosphate (CTP) synthetases also have end-gate-like residues.^{32,33} For instance, in GMP, like PurL, the end-gate residue, which is glutamate, also controls both glutaminase and synthetase activities and any perturbation of this residue resulted in complete loss of activity.³³ Therefore, it appears that systems where end gates are present maintain a tighter control on ammonia production.

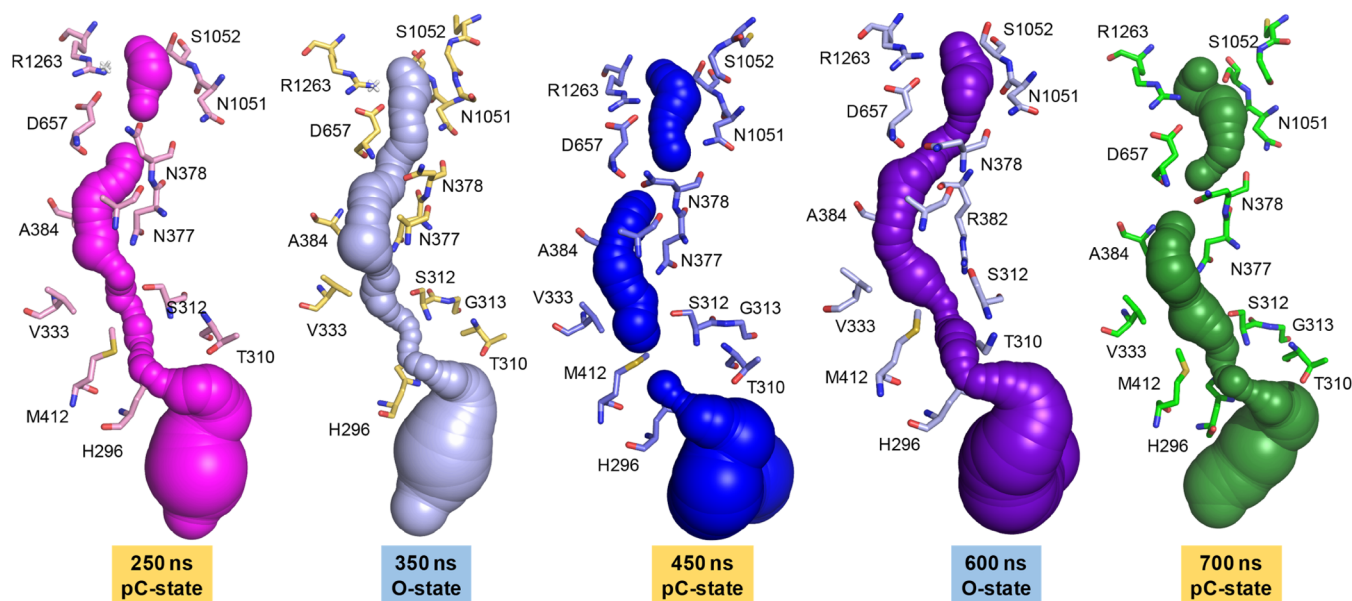


Figure 7. Pulsating transient ammonia channel. Breathing motion of the tunnel over the length of the simulation is highlighted using the CAVER3.0 PyMOL plugin. The channel opens and partially closes via synchronous motion of the bottleneck residues. The snapshots at 250, 450, and 700 ns representing the partially closed tunnel state “pC” and at 350 and 600 ns representing the open (tunnel) state “O” are shown. The partially closed and open tunnels are highlighted with spheres.

Additionally, in the case of PurL, the gating controls and catalytic controls are intertwined as the gating residue H296 is also an integral catalytic residue involved in proton abstraction from FGAR for iminophosphate intermediate formation at the FD-site (Scheme S2). Therefore, the PurL system seems to be an example where strong coupling exists between the two reaction centers and the whole communication network rests on substrate entry and gating at the synthetase site.

Ammonia Tunnel Signaling Network. R1263 is universally conserved in all FGAM synthetases (Figure S2), and comparison reveals that in class-I GATs the mouth-gate network is analogous to that observed in PurL. In all of these systems, at the ammonia exit site, a positively charged residue that forms a salt bridge with another acidic signaling residue (D657 in PurL) passes the communication to the adjacent coupled reaction site. For instance, we noticed that, similar to PurL, class-I GATs such as IGPS³⁴ and CPS¹⁵ also possess K196–D358 and K202–D258 residue pairs, respectively. Even class-II GATs such as phosphoribosyl pyrophosphate amidotransferase (PPAT),³⁵ glutamate synthetase (GltS),³⁶ and glucosamine-6P synthase (GlmS)³⁷ harbor this conserved residue pair, and this reasserts that the mode of signal transfer is most probably common across all GATs. A careful analysis of the crystal structures, mutagenesis, and MD studies indicates that it is the orientation of D657 that plays a central role in coordination of downstream relay. It is the degree of perturbation of D657 that affects the FGAM synthetase activity. Both the replacement of R1263 by a methionine that in turn disturbs the orientation of D657 (Figure S5B) and the D657A mutant exhibit moderate loss of signaling with effects percolating down to the FD-site as indicated by the crystal structure of D657A (Figure S6). However, the R1263D mutation is extremely debilitating to FGAM synthetase activity (Figures 2C and S4C and Table 1) as, most likely, this mutation not only disrupts the salt bridge pair but also results in repulsion of the nearby D657, which probably adopts a conformation that disturbs the pulsating tunnel architecture

and results in complete blockage of the signal. The cross-correlation analysis corroborates this observation as D657 was found to be a centrally connected residue (Figure S12). It shows a high correlation to the mouth-gate via R1263, the tunnel-lining residues, end-gate, and the allosteric C-loop network, indicating that positioning of D657 is paramount for communication.

Another important observation was the control of ammonia hydrolysis by N1051 in PurL, which influences the positioning of the central glycine residue, which is involved in stabilization of the anionic transition state. It has been well documented that an oxyanion hole is a dynamic feature that is transiently formed only during the progress of glutamine hydrolysis.^{21,38,39} Other GATs such as CPS, PPAT, GltS, and GlmS also harbor this asparagine residue, which in these systems is directly incorporated inside the oxyanion strand itself. However, in PurL and IGPS, this residue is present in an adjacent loop and indirectly controls the oxyanion hole conformation via dynamic interaction. MD simulations of the PurL system showed that the conserved glycine residue (G1092 in PurL) flips inward and creates an environment conducive for oxyanion hole formation.²⁴ We were experimentally able to observe this rare conformation in the N1051A mutant crystal structure (Figure 4B,C). In PurL, this residue along with D657 is also involved in the formation of the transient ammonia tunnel. N1051 is situated diametrically opposite to D657 and forms the other wall of the ammonia tunnel (Figure 3A). MD analysis shows that N1051 plays a crucial role in tunnel pulsation and in downstream signaling via controlling its hydrogen-bonding status with N377, a key tunnel-lining residue that forms the aperture of the vacillating tunnel (Figure 3B).

Proposed Model for the Catalytic Cycle. In conclusion, taking together the experimental and simulation data, a comprehensive catalytic cycle model is proposed that explains the complex allostery connecting the two reactions in PurL. The model represents four states of the enzyme (Figure 8). In

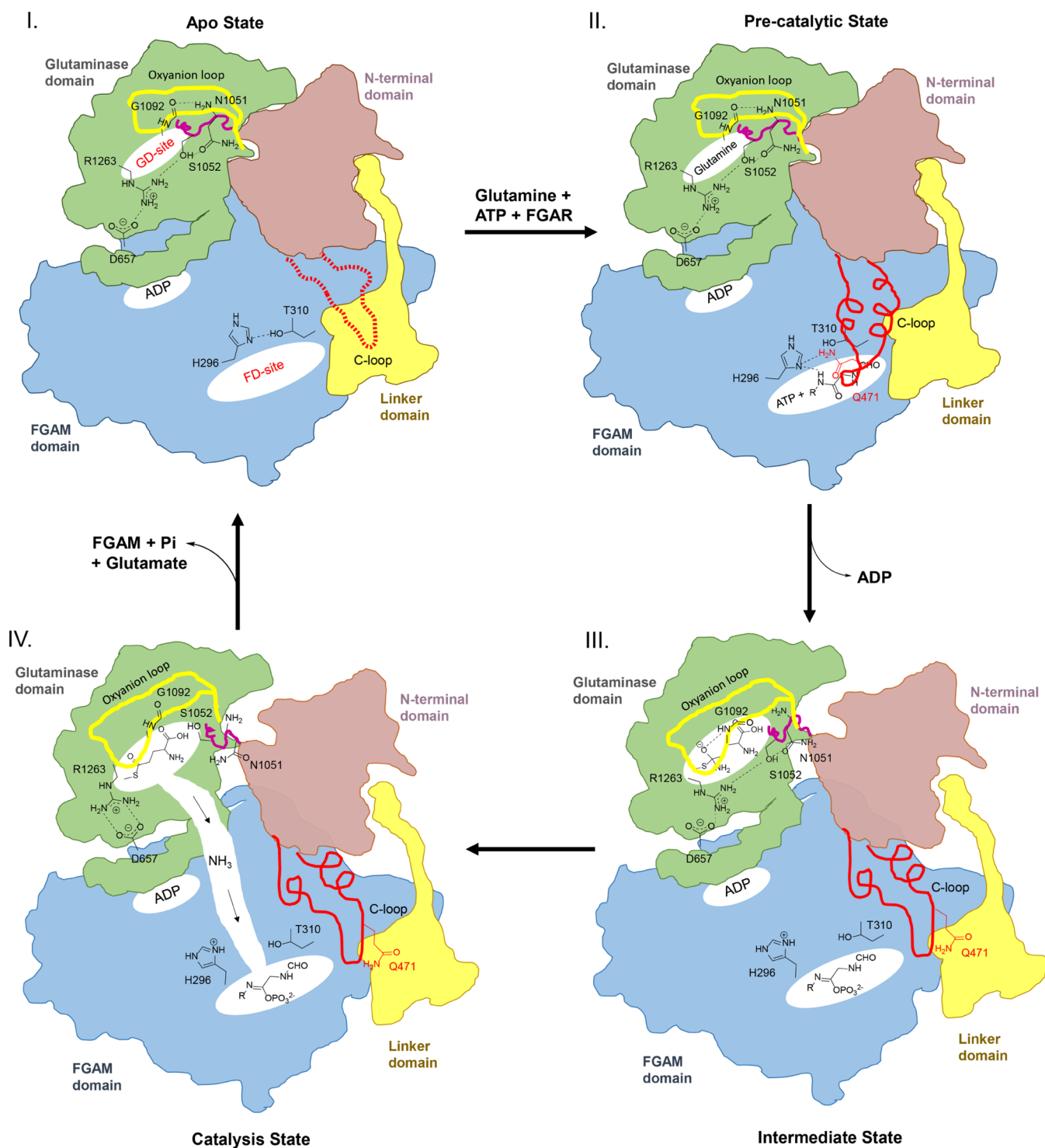


Figure 8. Model proposed for the allosteric signal transmission mechanism in PurL. State I, Apo state, represents the enzyme in the resting state, wherein no substrates are present. In this state, the ammonia channel is closed and the C-loop is disordered. Both the gates are in the closed configuration. State II represents the precatalytic state, wherein all of the substrates, glutamine in the G-site and FGAR and ATP in the F-site, are present and the C-loop adopts an ordered closed conformation capping the F-site. State III represents the intermediate state, wherein the rearrangement of the C-loop to a partially open state with a concomitant motion of the NTD and GD occurs. The end-gate opens, which further leads to the rearrangement of the oxyanion loop via the signaling loop residues. In state IV, catalysis state, the ammonia channel is fully formed. Glutamine hydrolysis at the G-site leads to the formation of ammonia that travels to the F-site, yielding the product FGAM. Here, the mouth-gate opens and closes multiple times, resulting in a breathing motion that transverses along the length of the ammonia tunnel.

state I, the enzyme is in the resting state, where the C-loop is disordered and the oxyanion loop is in an unproductive conformation (Figure 8). This state signifies a GD state with basal activity. Here, important loops that are essential for

crosstalk are flexible and do not take on defined conformations. State II signifies the entry of substrates FGAR and ATP that triggers ordering of the C-loop via interaction with FGAR (Figure 8). The C-loop additionally interacts with the gating

residue H296 via Q471. The end-gate network becomes activated, and the importance of this gate comes to the limelight as any perturbation of this gate completely halts the signal. Here, it is paramount to note that it is only FGAR entry and not ATP that triggers closure of the C-loop. The crystal structure where only ATP is bound (PDB-ID 3UMM) does not show any loop ordering,¹⁹ whereas the crystal structure where only FGAR is complexed (PDB-ID 2HS3) has an ordered C-loop.¹⁸ At this stage, the iminophosphate intermediate is generated by the attack of the δ -carbonyl group of the formylglycinamide side chain of FGAR to the γ -phosphate of ATP. The iminophosphate intermediate formation is evident from the two facts. First, PurL belongs to the ATP-grasp superfamily of enzymes that are proposed to undergo amination via iminophosphate formation.^{18,27} Second, a previously performed O¹⁸-labeled FGAR exchange experiment shows the quantitative transfer of labeled O¹⁸ to the released phosphate group during FGAM production, which is attributed to be possible only via the iminophosphate intermediate.⁴⁰ This γ -phosphate transfer is facilitated by abstraction of the proton via gating residue H296 from the adjacent $-\text{NH}-$ group of the formylglycinamide chain (Scheme S2). The intermediate formation introduces flipping of H296, resulting in opening of the end-gate. The end-gate opens and releases the C-loop that was tethered to the gate via H296–Q471 hydrogen-bonding interaction. The disruption of this interaction activates the allosteric switch. In stage III (Figure 8), a cascade of rearrangements is initiated, starting with the partial unfolding of the C-loop, creating a dynamic interface with the NTD.²⁴ The NTD then rotates by 8°, shifting toward the FD and moving away from the GD.²⁴ This motion releases the oxyanion loop (state III; Figure 8) and also opens up a passage for glutamine entry, priming the GD-site for ammonia production. This is the state where the GD-site is activated to produce ammonia. The restructuring of the hydrogen-bonding network at the mouth-gate along with the rearrangement in the oxyanion loop serves as a cue, and this information is transmitted to signaling residues D657 and N1051 that initiate mouth-gate opening and formation of the transient ammonia tunnel (state IV; Figure 8). The ammonia then traverses across the length of the protein and reaches the FD-site, wherein the nucleophilic attack by ammonia aided by H296 results in the formation of product FGAM. The catalytic cycle is complete and ready for the next round. Overall, we believe that the complex interaction relay system between two coupled reaction centers, presented here, where a dynamic allosteric switch gives rise to a pulsating ammonia tunnel, regulated by a dual gating network is an example of a biological system that has been fine-tuned to achieve perfection. This system represents an evolved apparatus for precise control of sequential chemical reactions with reactive intermediates.

METHODS

Sequence Conservation Analysis. Structure-based sequence conservation analysis was performed on large PurL (using PDB-ID 1T3T) and on smPurL and PurQ subunits of the PurSLQ complex (using PDB-ID 3D54) in the ConSurf online server available at <http://consurf.tau.ac.il>²⁵ (see details in Materials and Methods, Supporting Information (SI)).

Cloning, Expression, Purification, and Structure Determination. Mutants at the mouth and end region of the channel in PurL were designed by site-directed mutagenesis (SDM) and overlap extension polymerase chain

reaction (PCR) using previously reported methods.¹⁶ Crystals of mutants R1263A, N1051A, S1052D, D657A, and H296A were obtained by a hanging drop vapor diffusion method at 298 K, in the standard condition of the native enzyme, i.e., in 2 M (NH₄)₂SO₄.¹⁶ X-ray crystallographic studies were performed for the structure determination, for which the structure models were built using molecular replacement selecting the native PurL structure (PDB-ID 1T3T) as a model (see details in Materials and Methods, SI). Crystallographic data statistics are reported in Table S2. Circular dichroism (CD) spectroscopy was performed to determine the secondary structure content of all of the mutants using a JASCO J-815 CD spectrometer.

Activity Assay and Isothermal Calorimetry. Glutamate and FGAM production and leaky ammonia activities were determined using previously reported protocols⁴¹ (see details in Materials and Methods, SI). To determine the binding affinity of PurL mutants with glutamine, experiments were performed using MicroCal iTC₂₀₀ (GE Healthcare) (see details in Materials and Methods, SI).

Modeling, Molecular Dynamics (MD) Simulation, and Cross-Correlation Analysis. Previously reported MD simulation trajectories (see details in Materials and Methods, SI) were reanalyzed, while for Q471A mutant, 750 ns simulation was run in the present study. For native PurL, the computational structural model was generated from the crystal structure of the PurL mutant having the closed C-loop conformation (PDB-ID 6JTA),²⁴ while for Q471A, the mutant structure was generated by mutating the Q471 residue with alanine in the same structure having a closed C-loop conformation. To track the correlation between the residue pair motions of gating, channel-lining, C-loop, and NTD residues relative to each other over the simulation length, cross-correlation analysis was performed. The selected residue pair distances were given as input and Pearson's correlation coefficients were calculated using the "corrcoef" tool in MATLAB⁴² by the formula

$$\rho(A, B) = \text{cov}(A, B) / \sigma_A \sigma_B$$

where $\text{cov}(A, B)$ is the covariance of two independent variables A and B and σ_A and σ_B are the standard deviations of variables A and B , respectively. A correlation coefficient matrix is finally generated for each pairwise variable combination and plotted in ImageJ for visualization.

ASSOCIATED CONTENT

Supporting Information

The Supporting Information is available free of charge at <https://pubs.acs.org/doi/10.1021/acscatal.1c05521>.

C-loop opening (Video v1) (MPG)

Gate opening and channel formation (Video v2) (MP4)

Mouth-gate network (Video v3) (MPG)

End-gate network (Video v4) (MPG)

Complete experimental procedures; crystallographic data statistics (Table S1); thermodynamic parameters (Table S2); global motions in PurL, sequence conservation, and secondary structure analysis, CD, kinetic and ITC profiles, FD-site analysis, signal transmission at the C-loop and end-gate region and to the oxyanion loop, distorted motion of the C-loop in Q471, pulsating transient ammonia channel, and cross-correlation analysis (Figures S1–S12); and formation of

oxyanion tetrahedral transition complex and role of H296 in FGAR to FGAM conversion (Schemes S1 and S2) (PDF)

AUTHOR INFORMATION

Corresponding Author

Ruchi Anand – Department of Chemistry, Indian Institute of Technology Bombay, Mumbai 400076, India; orcid.org/0000-0002-2045-3758; Email: ruchi@chem.iitb.ac.in

Authors

Nandini Sharma – Department of Chemistry, Indian Institute of Technology Bombay, Mumbai 400076, India; orcid.org/0000-0003-4053-2186

Sukhwinder Singh – Department of Chemistry, Indian Institute of Technology Bombay, Mumbai 400076, India; orcid.org/0000-0002-2269-3640

Ajay S. Tanwar – Department of Chemistry, Indian Institute of Technology Bombay, Mumbai 400076, India

Jagannath Mondal – Centre for Interdisciplinary Science, Tata Institute of Fundamental Research, Hyderabad 500107, India; orcid.org/0000-0003-1090-5199

Complete contact information is available at: <https://pubs.acs.org/10.1021/acscatal.1c05521>

Author Contributions

[§]S.S. and A.S.T. contributed equally to this work. N.S. performed all of the experiments including molecular cloning, protein purification, activity assays, isothermal calorimetry, circular dichroism, X-ray crystallography, and MD data analysis and wrote the manuscript. S.S. performed molecular cloning, protein purification, activity assays, circular dichroism, and X-ray crystallography. A.S.T. performed molecular cloning, protein purification, activity assays, circular dichroism, and X-ray crystallography. J.M. provided the computational facility for running MD simulations at TIFR, Hyderabad, carried out MD simulations, and helped in MD analysis. R.A. provided the lab facility for performing all of the experimental work, helped in data interpretation, and wrote the manuscript with input from all of the authors.

Notes

The authors declare no competing financial interest.

ACKNOWLEDGMENTS

The authors thank Prof. Ishita Sengupta, Prof. Arindam Chowdhury, and the reviewers of the manuscript for giving their helpful suggestions to improve the manuscript. The authors also acknowledge beamline BM14, the European Synchrotron Radiation Facility (ESRF), Grenoble, France, the National Institute of Immunology (NII), Delhi, India, and IIT Bombay for providing XRD facility for initial crystallization screening and data collection. The authors also acknowledge the Department of Science and Technology (DST), Government of India, grant number DST/INT/SOUTH AFRICA/P-04/2014 for funding. NS acknowledges the University Grant Commission (UGC) for providing fellowship. SS acknowledges the Council of Scientific and Industrial Research (CSIR) for the fellowship.

REFERENCES

- (1) Marques, S. M.; Daniel, L.; Buryska, T.; Prokop, Z.; Brezovsky, J.; Damborsky, J. Enzyme Tunnels and Gates As Relevant Targets in Drug Design. *Med. Res. Rev.* **2017**, *37*, 1095–1139.
- (2) Risler, J.-L.; Brézellec, P.; Pasek, S. Gene fusion/fission is a major contributor to evolution of multi-domain bacterial proteins. *Bioinformatics* **2006**, *22*, 1418–1423.
- (3) Cheng, X.-Y.; Huang, W.-J.; Hu, S.-C.; Zhang, H.-L.; Wang, H.; Zhang, J.-X.; Lin, H.-H.; Chen, Y.-Z.; Zou, Q.; Ji, Z.-L. A global characterization and identification of multifunctional enzymes. *PLoS One* **2012**, *7*, No. e38979.
- (4) Gunasekaran, K.; Ma, B.; Nussinov, R. Is allosteric an intrinsic property of all dynamic proteins? *Proteins: Struct., Funct., Bioinf.* **2004**, *57*, 433–443.
- (5) Tzeng, S.-R.; Kalodimos, C. G. Allosteric inhibition through suppression of transient conformational states. *Nat. Chem. Biol.* **2013**, *9*, 462.
- (6) Goodey, N. M.; Benkovic, S. J. Allosteric regulation and catalysis emerge via a common route. *Nat. Chem. Biol.* **2008**, *4*, 474.
- (7) Liu, J.; Nussinov, R. Allosteric: An Overview of Its History, Concepts, Methods, and Applications. *PLoS Comput. Biol.* **2016**, *12*, No. e1004966.
- (8) Massière, F.; Badet-Denisot, M. A. The mechanism of glutamine-dependent amidotransferases. *Cell. Mol. Life Sci.* **1998**, *54*, 205–222.
- (9) Rauschel, F. M.; Thoden, J. B.; Holden, H. M. The Amidotransferase Family of Enzymes: Molecular Machines for the Production and Delivery of Ammonia. *Biochemistry* **1999**, *38*, 7891–7899.
- (10) Sheik Amamuddy, O.; Veldman, W.; Manyumwa, C.; Khairallah, A.; Agajanian, S.; Oluyemi, O.; Verkhivker, M. G.; Tastan Bishop, Ö. Integrated Computational Approaches and Tools for Allosteric Drug Discovery. *Int. J. Mol. Sci.* **2020**, *21*, No. 847.
- (11) Gora, A.; Brezovsky, J.; Damborsky, J. Gates of enzymes. *Chem. Rev.* **2013**, *113*, 5871–5923.
- (12) Pavlova, M.; Klvana, M.; Prokop, Z.; Chaloupkova, R.; Banas, P.; Otyepka, M.; Wade, R. C.; Tsuda, M.; Nagata, Y.; Damborsky, J. Redesigning dehalogenase access tunnels as a strategy for degrading an anthropogenic substrate. *Nat. Chem. Biol.* **2009**, *5*, 727–733.
- (13) Endrizzi, J. A.; Kim, H.; Anderson, P. M.; Baldwin, E. P. Mechanisms of Product Feedback Regulation and Drug Resistance in Cytidine Triphosphate Synthetases from the Structure of a CTP-Inhibited Complex. *Biochemistry* **2005**, *44*, 13491–13499.
- (14) Amaro, R. E.; Myers, R. S.; Davissón, V. J.; Luthey-Schulten, Z. A. Structural Elements in IGP Synthase Exclude Water to Optimize Ammonia Transfer. *Biophys. J.* **2005**, *89*, 475–487.
- (15) Fan, Y.; Lund, L.; Shao, Q.; Gao, Y.-Q.; Raushel, F. M. A Combined Theoretical and Experimental Study of the Ammonia Tunnel in Carbamoyl Phosphate Synthetase. *J. Am. Chem. Soc.* **2009**, *131*, 10211–10219.
- (16) Anand, R.; Hoskins, A. A.; Stubbe, J.; Ealick, S. E. Domain Organization of *Salmonella typhimurium* Formylglycinamide Ribonucleotide Amidotransferase Revealed by X-ray Crystallography. *Biochemistry* **2004**, *43*, 10328–10342.
- (17) Anand, R.; Hoskins, A. A.; Bennett, E. M.; Sintchak, M. D.; Stubbe, J.; Ealick, S. E. A Model for the *Bacillus subtilis* Formylglycinamide Ribonucleotide Amidotransferase Multiprotein Complex. *Biochemistry* **2004**, *43*, 10343–10352.
- (18) Morar, M.; Anand, R.; Hoskins, A. A.; Stubbe, J.; Ealick, S. E. Complexed Structures of Formylglycinamide Ribonucleotide Amidotransferase from *Thermotoga maritima* Describe a Novel ATP Binding Protein Superfamily. *Biochemistry* **2006**, *45*, 14880–14895.
- (19) Tanwar, A. S.; Morar, M.; Panjekar, S.; Anand, R. Formylglycinamide ribonucleotide amidotransferase from *Salmonella typhimurium*: role of ATP complexation and the glutaminase domain in catalytic coupling. *Acta Crystallogr., Sect. D: Biol. Crystallogr.* **2012**, *68*, 627–636.
- (20) Morar, M.; Hoskins, A. A.; Stubbe, J.; Ealick, S. E. Formylglycinamide Ribonucleotide Amidotransferase from Thermo-

toga maritima: Structural Insights into Complex Formation. *Biochemistry* **2008**, *47*, 7816–7830.

(21) Huang, X.; Holden, H. M.; Raushel, F. M. Channeling of Substrates and Intermediates in Enzyme-Catalyzed Reactions. *Annu. Rev. Biochem.* **2001**, *70*, 149–180.

(22) Raushel, F. M.; Thoden, J. B.; Holden, H. M. Enzymes with Molecular Tunnels. *Acc. Chem. Res.* **2003**, *36*, 539–548.

(23) Wheeldon, I.; Minteer, S. D.; Banta, S.; Barton, S. C.; Atanassov, P.; Sigman, M. Substrate channelling as an approach to cascade reactions. *Nat. Chem.* **2016**, *8*, 299.

(24) Sharma, N.; Ahalawat, N.; Sandhu, P.; Strauss, E.; Mondal, J.; Anand, R. Role of allosteric switches and adaptor domains in long-distance cross-talk and transient tunnel formation. *Sci. Adv.* **2020**, *6*, No. eaay7919.

(25) Martz, E.; Glaser, F.; Mayrose, I.; Landau, M.; Ben-Tal, N.; Pupko, T.; Rosenberg, Y. ConSurf 2005: the projection of evolutionary conservation scores of residues on protein structures. *Nucleic Acids Res.* **2005**, *33*, W299–W302.

(26) Schendel, F. J.; Mueller, E. J.; Stubbe, J.; Shiau, A.; Smith, J. M. Formylglycinamide ribonucleotide synthetase from *Escherichia coli*: cloning, sequencing, overproduction, isolation, and characterization. *Biochemistry* **1989**, *28*, 2459–2471.

(27) Hoskins, A. A.; Anand, R.; Ealick, S. E.; Stubbe, J. The Formylglycinamide Ribonucleotide Amidotransferase Complex from *Bacillus subtilis*: Metabolite-Mediated Complex Formation. *Biochemistry* **2004**, *43*, 10314–10327.

(28) Semmelmann, F.; Hupfeld, E.; Heizinger, L.; Merkl, R.; Sterner, R. A Fold-Independent Interface Residue Is Crucial for Complex Formation and Allosteric Signaling in Class I Glutamine Amidotransferases. *Biochemistry* **2019**, *58*, 2584–2588.

(29) Rivalta, I.; Sultan, M. M.; Lee, N.-S.; Manley, G. A.; Loria, J. P.; Batista, V. S. Allosteric pathways in imidazole glycerol phosphate synthase. *Proc. Natl. Acad. Sci. U.S.A.* **2012**, *109*, No. E1428.

(30) Chovancova, E.; Pavelka, A.; Benes, P.; Strnad, O.; Brezovsky, J.; Kozlikova, B.; Gora, A.; Sustr, V.; Klvana, M.; Medek, P.; Biedermannova, L.; Sochor, J.; Damborsky, J. CAVER 3.0: A Tool for the Analysis of Transport Pathways in Dynamic Protein Structures. *PLoS Comput. Biol.* **2012**, *8*, No. e1002708.

(31) Stank, A.; Kokh, D. B.; Fuller, J. C.; Wade, R. C. Protein Binding Pocket Dynamics. *Acc. Chem. Res.* **2016**, *49*, 809–815.

(32) Goto, M.; Omi, R.; Nakagawa, N.; Miyahara, I.; Hirotsu, K. Crystal Structures of CTP Synthetase Reveal ATP, UTP, and Glutamine Binding Sites. *Structure* **2004**, *12*, 1413–1423.

(33) Ballut, L.; Violot, S.; Shivakumaraswamy, S.; Thota, L. P.; Sathya, M.; Kunala, J.; Dijkstra, B. W.; Terreux, R.; Haser, R.; Balaram, H.; Aghajari, N. Active site coupling in *Plasmodium falciparum* GMP synthetase is triggered by domain rotation. *Nat. Commun.* **2015**, *6*, No. 8930.

(34) Chaudhuri, B. N.; Lange, S. C.; Myers, R. S.; Davisson, V. J.; Smith, J. L. Toward Understanding the Mechanism of the Complex Cyclization Reaction Catalyzed by Imidazole Glycerolphosphate Synthase: Crystal Structures of a Ternary Complex and the Free Enzyme. *Biochemistry* **2003**, *42*, 7003–7012.

(35) Krahn, J. M.; Kim, J. H.; Burns, M. R.; Parry, R. J.; Zalkin, H.; Smith, J. L. Coupled Formation of an Amidotransferase Interdomain Ammonia Channel and a Phosphoribosyltransferase Active Site. *Biochemistry* **1997**, *36*, 11061–11068.

(36) van den Heuvel, R. H. H.; Svergun, D. I.; Petoukhov, M. V.; Coda, A.; Curti, B.; Ravasio, S.; Vanoni, M. A.; Mattevi, A. The Active Conformation of Glutamate Synthase and its Binding to Ferredoxin. *J. Mol. Biol.* **2003**, *330*, 113–128.

(37) Mouilleron, S.; Badet-Denisot, M.-A.; Golinelli-Pimpaneau, B. Glutamine Binding Opens the Ammonia Channel and Activates Glucosamine-6P Synthase. *J. Biol. Chem.* **2006**, *281*, 4404–4412.

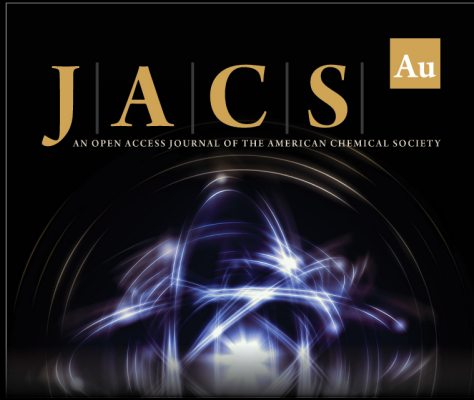
(38) Anderson, K. S. [6] Fundamental Mechanisms of Substrate Channeling. *Methods in Enzymology*; Academic Press, 1999; pp 111–145.

(39) Miles, E. W.; Rhee, S.; Davies, D. R. The Molecular Basis of Substrate Channeling. *J. Biol. Chem.* **1999**, *274*, 12193–12196.

(40) Schendel, F. J.; Mueller, E.; Stubbe, J.; Shiau, A.; Smith, J. M. Formylglycinamide ribonucleotide synthetase from *Escherichia coli*: cloning, sequencing, overproduction, isolation, and characterization. *Biochemistry* **1989**, *28*, 2459–2471.


(41) Schendel, F. J.; Stubbe, J. Substrate specificity of formylglycinamide synthetase. *Biochemistry* **1986**, *25*, 2256–2264.


(42) MathWorks Inc. *MATLAB: The Language of Technical Computing: Computation, Visualization, Programming: Installation Guide for UNIX*, version 5; Math Works Inc.: Natwick, 1996.



JACS Au
AN OPEN ACCESS JOURNAL OF THE AMERICAN CHEMICAL SOCIETY

Editor-in-Chief
Prof. Christopher W. Jones
Georgia Institute of Technology, USA

Open for Submissions 

pubs.acs.org/jacsau  ACS Publications
Most Trusted. Most Cited. Most Read.